Primordial neurosecretory apparatus identified in the choanoflagellate *Monosiga brevicollis*

Pawel Burkhardt[a,1], Christian M. Stegmann[b,2], Benjamin Cooper[c], Tobias H. Kloepper[d], Cordelia Imig[c], Frédérique Varoqueaux[c,e], Markus C. Wahl[b,f], and Dirk Fasshauer[a,g,3]

[a]Research Group Structural Biochemistry, Department of Neurobiology, and [b]Research Group X-Ray Crystallography, Max Planck Institute for Biophysical Chemistry, 37077 Göttingen, Germany; [c]Department of Molecular Neurobiology, Max Planck Institute of Experimental Medicine, 37075 Göttingen, Germany; [d]Medical Research Council Laboratory of Molecular Biology, Cambridge CB2 0QH, United Kingdom; [e]Center for Molecular Physiology of the Brain, 37075 Göttingen, Germany; [f]AG Strukturbiochemie, Institut für Chemie und Biochemie, Freie Universität Berlin, 14195 Berlin, Germany; and [g]Department of Cellular Biology and Morphology, University of Lausanne, 1005 Lausanne, Switzerland

SNARE protein-driven secretion of neurotransmitters from synaptic vesicles is at the center of neuronal communication. In the absence of the cytosolic protein Munc18-1, synaptic secretion comes to a halt. Although it is believed that Munc18-1 orchestrates SNARE complexes, its mode of action is still a matter of debate. In particular, it has been challenging to clarify the role of a tight Munc18/syntaxin 1 complex, because this interaction interferes strongly with syntaxin's ability to form a SNARE complex. In this complex, two regions of syntaxin, the *N*-peptide and the remainder in closed conformation, bind to Munc18 simultaneously. Until now, this binary complex has been reported for neuronal tissues only, leading to the hypothesis that it might be a specialization of the neuronal secretion apparatus. Here we aimed, by comparing the core secretion machinery of the unicellular choanoflagellate *Monosiga brevicollis* with that of animals, to reconstruct the ancestral function of the Munc18/syntaxin1 complex. We found that the Munc18/syntaxin 1 complex from *M. brevicollis* is structurally and functionally highly similar to the vertebrate complex, suggesting that it constitutes a fundamental step in the reaction pathway toward SNARE assembly. We thus propose that the primordial secretion machinery of the common ancestor of choanoflagellates and animals has been co-opted for synaptic roles during the rise of animals.

Neurons, the building blocks of the nervous system, are highly specialized for fast information transmission, which takes place in the form of vesicular neurotransmitter release at specialized junctions, the chemical synapses. Synapses evolved early in animal evolution, and relatively primitive nervous systems can be found in early branching animals, such as jellyfish (1, 2). By contrast, sponges (3) or the placozoan *Trichoplax adhaerens* (4), appear not to be equipped with bona fide synapses, yet possess several factors related to synaptic function. Hence, it is possible that central features of synaptic transmission evolved early in animal evolution, possibly during the transition to multicellularity.

Choanoflagellates, a group of mostly single-celled eukaryotes that possess a single posterior flagellum surrounded by a collar of actin-based tentacles, are thought to be the closest known sister group to animals (5–8). Although a long period separates the choanoflagellate and animal lineages, it is possible that choanoflagellates have remained similar to the unicellular organism from which all animals evolved (e.g., refs. 7–13). However, it remains unclear which molecular mechanism of the unicellular precursor was fundamental for the development of the neuronal communication apparatus (14)?

To address this matter we focused on a key feature of synapses, the rapid discharge of neurotransmitter-loaded vesicles upon fusion with the presynaptic plasma membrane. In vertebrates, this process is mediated by the neurosecretory soluble NSF attachment protein receptors (SNARE) proteins synaptobrevin 2, syntaxin 1, and SNAP-25. Their assembly between the opposing membranes is thought to drive membrane fusion (15). SNARE function is tightly regulated by Munc18-1, a member of

the conserved Sec1/Munc18 (SM) protein family. In the absence of Munc18-1, neurotransmitter release is blocked completely (16–18); note that the homologous factor is referred to as Rop1 in *Drosophila melanogaster* and Unc18 in *Caenorhabitis elegans*. The biochemical correlate(s) underlying this positive genetic role remain a matter of debate (e.g., reviewed in refs. 19–22 but see also ref. 23). In brief, it has been challenging to integrate the role of a very tight Munc18/syntaxin 1 complex, because the grip of Munc18 strongly interferes with syntaxin's ability to form a SNARE complex (23–25). It was therefore suggested that the Munc18/syntaxin 1 complex is not universal but plays a special role during neuronal secretion only (20, 21, 26, 27). So far, comparative studies on the other vertebrate Munc18 isoforms, Munc18-2 and Munc18-3, or on the *Sacharomyces cerevisiae* homolog Sec1 have not been able to clarify this conundrum (28–32). Thus, we decided to tackle the question about the role of the tight Munc18/syntaxin 1 complex from a new angle by comparing the workings of the homologous secretion machinery of the choanoflagellate *Monosiga brevicollis* with that of animals. Here, we report that *M. brevicollis* expresses a Munc18 homolog and find that all three secretory SNARE proteins and Munc18 are confined to the apical pole. Further, the mode of interaction of Munc18 and syntaxin 1 from *M. brevicollis* strikingly resembles that of their animal homologs. Finally, the crystal structure of the *M. brevicollis* Munc18/syntaxin 1 complex revealed that this high-affinity interaction involves contacts between the *N*-peptide of syntaxin 1 and its remainder in closed conformation, as it does in the rat. This binding behavior shows that the configuration of the Munc18/syntaxin 1 complex was already in place in the last common ancestor of choanoflagellates and animals.

Results

M. brevicollis Is Equipped with a Single Set of Synapse-Like Core Secretion Proteins. The genome of the choanoflagellate *M. brevicollis* contains a single set of secretory SNARE proteins (33) and a unique Munc18 homolog, closely related to the ones involved in regulated secretion in animals (Fig. 1). These distributions suggest that the last common ancestor of choanoflagellates and ani-
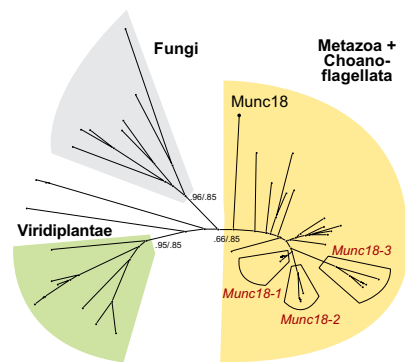
EVOLUTION

Fig. 1. Schematic outline of a phylogenetic tree of the SM protein Munc18 demonstrates that the core machinery of the secretory apparatus of *M. brevicollis* is closely related to animals. Detailed versions of the Munc18 tree and also of the SNAP-25 and syntaxin1 trees are shown in Fig. S1. The major eukaryotic lineages are emphasized by different colors, expansions in the vertebrate lineage are indicated. In addition, the position of Munc18 from *M. brevicollis* (Munc18) is shown. Whereas *M. brevicollis* possesses only one Munc18 homolog expansion of Munc18-like factors occurred in vertebrates, giving rise to the three isoforms Munc18-1, -2, and -3. The labels on the major branches represent the Likelihood Mapping (*Left*) and almost unbiased (AU) support values (*Right*).

mals was equipped with only one set of core secretion proteins that likely bore a close resemblance to the factors found in the genome of *M. brevicollis*.

Secretory Components Are Confined to the Apical Pole of *M. brevicollis*. Although choanoflagellate genomes can assist in reconstructing the genetic tool kit of the common ancestor of choanoflagellates and animals, their morphology may allow a glimpse at the features of the early animal cell. Indeed, striking morphological similitudes between choanoflagellates and sponge choanocytes have been noted already in the middle of the 19th century (ref. 9; reviewed in ref. 34). The close relationship between choanoflagellates and

animals has been confirmed by phylogenetic analysis (7, 8, 10, 11). Hence, studying the localization and interactions of *M. brevicollis* proteins could shed light on their original role.

We assessed the subcellular localization of these secretory proteins in *M. brevicollis* by immunostaining. To this end, we raised polyclonal antibodies against the soluble region of synaptobrevin 1 from *M. brevicollis*. In addition, we found that several antibodies originally raised against the rat proteins syntaxin 1a, SNAP-25, and Munc18-1 also specifically recognized their respective homologs from *M. brevicollis*. All four core components of the secretory machinery are confined to the posterior pole of the cell (Fig. 2A), a region that has been suggested to be involved in secretion (35). For example, in the derived lineage of loricate choanoflagellates, the building blocks of the lorica, so-called costal strips, are secreted within the circumfence of the collar base (7). At the ultrastructural level, the basic arrangement of organelles in *M. brevicollis* (Fig. 2B) resembles the arrangement reported for other choanoflagellates (e.g., refs. 35 and 36). At the posterior pole, the single Golgi apparatus is observed beneath the nucleus, and numerous vesicles of 75–200 nm in diameter are mostly directed to the rear end of the cell, close to the plasma membrane (Fig. 2B, *Right*).

Together these data are congruous with the notion that choanoflagellates possess a well-defined secretory machinery that, while relatively simple, may have served as the raw material for the evolution of the intricate machinery found in animal cells.

Conserved Properties of the Core Secretory Components of *M. brevicollis*. To study the interaction of the choanoflagellate proteins directly, we expressed the proteins in *E. coli*. We found that the three SNARE proteins form an SDS-resistant complex (Fig. 3A), as the neuronal SNARE complex from several different animal species do (37). The high stability of the core SNARE complex from *M. brevicollis* was confirmed by circular dichroism (CD) spectroscopy (Fig. 3B).

We next studied the interaction of the choanoflagellate Munc18 with the SNARE machinery. We first explored the canonical binary interaction between Munc18 and syntaxin 1
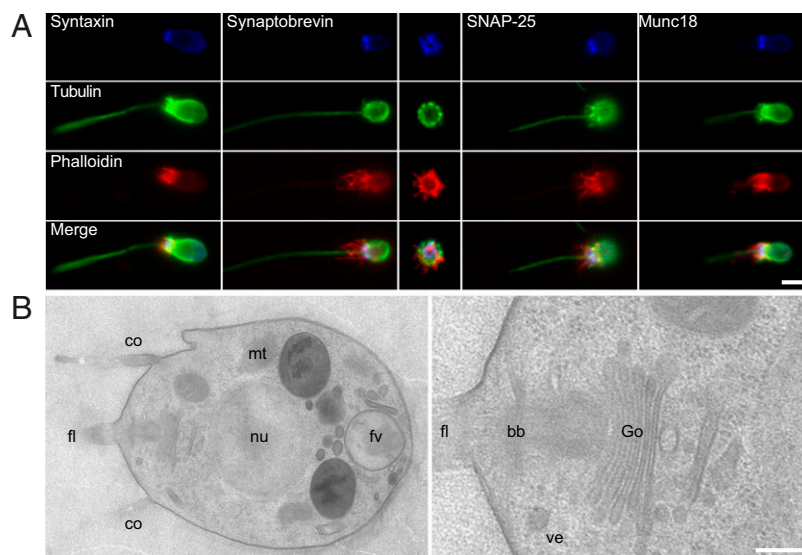
Fig. 2. SNAREs, Munc18, and the secretory apparatus in *M. brevicollis*. (*A*) Confocal micrographs illustrate immunolabelings for syntaxin 1, synaptobrevin, SNAP-25, or Munc18, all detected at the posterior (apical) pole of the cell. (*Center*) A cross-section image through the posterior pole shows a circular distribution of synaptobrevin. Colabeling of tubulin and actin allow for identifying the cell's cytoskeleton/architecture. (*B*) Ultrastructural investigation reveals the presence of the Golgi apparatus (Go) and associated clear vesicles (ve) at the posterior pole of the cell, near the root/basal body of the flagellum (fl) (*Right*). Note the presence of unrelated, heterogeneous large vesicles, most probably food vacuoles (fv), at the anterior pole (*Left*). The cell nucleus (nu), mitochondria (mt), and the collar (co) are indicated as well. (Scale bars: *A*, 1 μm; *B*, 500 nm.)

Fig. 3. The secretory SNARE proteins from *M. brevicollis* form a highly stable, SDS-resistant complex. (*A*) Approximately stoichiometric amounts of SNAP-25, syntaxin 1, and synaptobrevin from *R. norvegicus* or from *M. brevicollis* were mixed and incubated for 3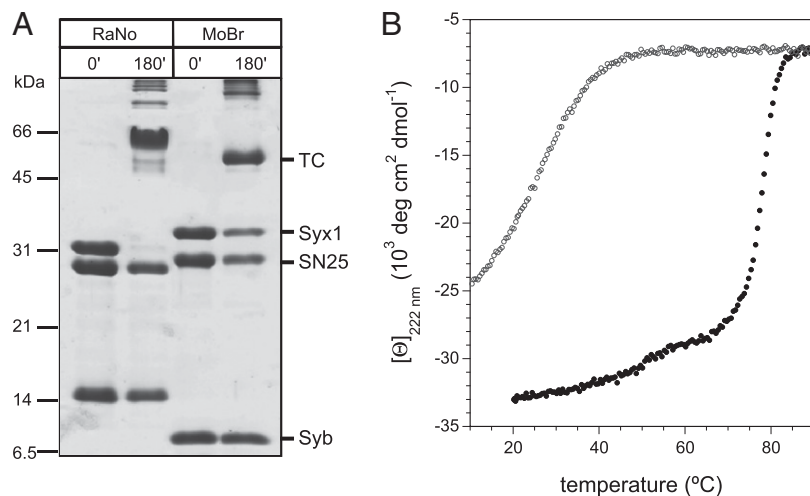 h at RT. Without prior boiling, the secretory SNARE proteins from both species form ternary SDS-resistant complexes (tc) as indicated (37). (*B*) The core SNARE complex from *M. brevicollis* exhibits a hysteresis in the unfolding and refolding transitions similar to the one found for the rat complex (41). The core SNARE complex consisting of Syx1 (200-279), Syb (1-75), and SNAP-25 was purified by ion exchange and measured in PBS buffer, pH 7.4. Unfolding of the α-helical complex occurred at $T_m \sim 80$ °C (black curve), whereas refolding was observable only at ≈ 50 °C (gray curve). The transitions were observed at 222 nm.

quantitatively by using isothermal titration calorimetry (ITC). We found that the entire cytosolic domain of syntaxin 1, Syx1 (1-279), binds to Munc18 with high affinity (K_d = 3.9 nM; Fig. 4 and Table 1). A comparable affinity has been determined for the interaction of Munc18-1 and syntaxin 1a from rat (23). In addition, the interaction between Munc18 and syntaxin 1 from *M. brevicollis* led to an increase in intrinsic fluorescence (Fig. S2*A*) similar to what has been observed for the rat homologs (23), corroborating that both complexes adopt a similar configuration (Fig. S2*B*). Of note, we found that rat Munc18-1 is able to bind to *M. brevicollis* syntaxin 1, albeit with reduced affinity (K_d = 80 nM; Fig. S3), confirming the close resemblance of the homologous pairs.

Two distinct regions of syntaxin 1a are known to contribute to the interaction with Munc18-1: The very N-terminal region, called the *N*-peptide, binds to the outer surface of Munc18-1's domain 1, whereas the remainder of the syntaxin molecule in a closed conformation binds to a clamp-like structure formed by the three domains of Munc18-1 (23). To test whether a similar configuration may play a role in the interaction of Munc18 and syntaxin 1 from *M. brevicollis*, we generated several deletion constructs of syntaxin 1. A syntaxin 1 variant, in which the first 19 residues were removed, Syx1 (20-279), showed a clearly reduced affinity to Munc18 ($K_d \sim 64$ nM), and a decrease in binding enthalpy ($\Delta\Delta H$ = 10.9 kJ/mol; Fig. 4 and Table 1). However, no binding was detected when the *N*-peptide alone, Syx1 (1–20), was

tested (Table 1 and Fig. S3). Thus, in *M. brevicollis* as in the rat, the *N*-peptide and the remaining portion of syntaxin 1 cooperate for high affinity binding to Munc18.

We then tested binding of Munc18 from *M. brevicollis* to fully assembled SNARE complexes containing different syntaxin constructs. We found that Munc18 binds to the SNARE complex containing Syx1 (1-279) with rather low affinity ($K_d \sim 570$ nM; Table 1 and Fig. S3), whereas no binding was detected between Munc18 and a SNARE complex containing syntaxin 1 bearing only its SNARE domain region [Syx1 (200-279)]. This ITC experiment indicates that in *M. brevicollis*, as in the rat (23), Munc18 does not interact significantly with the extended four-helix bundle SNARE complex.

Crystal Structure of the Munc18/Syntaxin 1 Complex from *M. brevicollis*. Altogether, our ITC analysis suggests a mode of interaction between Munc18 and secretory SNAREs from *M. brevicollis* very similar to that of the vertebrate homologs. To more precisely assess the degree of conservation, we then determined the structure of the complex from *M. brevicollis* by X-ray crystallography.

The crystal structure confirmed that two regions of syntaxin 1, the *N*-peptide and the remainder in closed conformation, bind to Munc18 simultaneously (Fig. 5). Very similar to the structure of the neuronal Munc18-1/syntaxin 1a complex, the *N*-peptide of the choanoflagellate syntaxin 1 binds to the outer surface of

Table 1. Thermodynamic parameters for Munc18/syntaxin 1 interactions from *M. brevicollis*

Munc18 interaction with	K_d, nM	$\Delta H°$, kcal/mole	n
Syx1 (1-279)	3.9 ± 0.6	−36.7 ± 0.2	0.91
Syx1 (1-265)	5.0 ± 0.9	−36.8 ± 0.3	0.95
Syx1 (1-242)	450.4 ± 77.3	−9.6 ± 0.6	0.94
Syx1 (1-199)	558.7 ± 88.6	−2.8 ± 0.3	0.92
Syx1 (1-20)	—	—	—
Syx1 (20-279)	64.1 ± 7.0	−25.8 ± 0.4	0.91
SNARE complex containing Syx1 (1-279)	571.4 ± 62.6	−3.0 ± 0.2	1.04
SNARE complex containing Syx1 (200-279)	—	—	—

The corresponding experimental ITC data are shown in Fig. S3. Note that no heat changes were detected when Syx1 (1-20) or the SNARE-complex containing Syx1 (200-279) were mixed with Munc18.
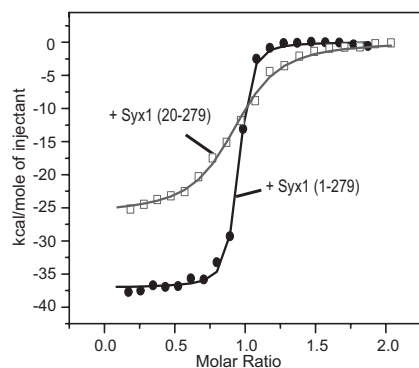
Fig. 4. Munc18 and syntaxin 1 from *M. brevicollis* interact with nanomolar affinity. Calorimetric titrations of syntaxin 1 into Munc18 from *M. brevicollis*. Syx1 (1-279) binds Munc18 with higher affinity and enthalpy than Syx1 (20-279), indicating that the *N*-peptide participates in binding. The graph displays the integrated areas normalized to the amount of the injectant (kcal·mol^{-1}) versus its molar ratio to Munc18. The solid lines represent the best fit to the data for a single binding site model. The raw data are shown in Fig. S3.

Munc18 domain 1, whereas the remainder of syntaxin 1 interacts with the concave surface formed by domains 1 and 3a of Munc18. In fact, the structures of the choanoflagellate Munc18/syntaxin 1 complex and rat Munc18-1/syntaxin 1a complex can be superimposed with an overall mainchain rmsd of 2.0 Å. Despite the close overall similarity there is a difference to note: The linker helix between syntaxin Habc and H3 domains of *M. brevicollis* adopts a slightly different conformation than observed in the rat crystal structure. This difference in orientation can be attributed to the lack of a salt bridge between Arg142 of the Hb
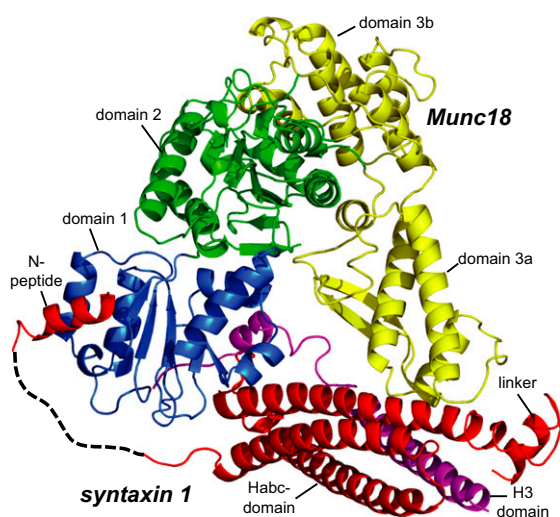

Fig. 5. Crystal structure of the Munc18/syntaxin 1 complex from *M. brevicollis*. Munc18 domain 1 is formed by residues 1–129, domain 2 by residues 130–237 and 477–616, and domain 3 by residues 238–476. Domain 3 can be further subdivided into a lower half (3a) and an upper half (3b). The domains of Munc18 are colored blue, green, and yellow, respectively. The *N*-peptide (residues 2–15), the Habc (residues 39–172), the linker helix (183-192) of syntaxin 1 are colored red, and the H3 region (residues 210–261) is colored purple. The dashed line represents residues 16–38 of syntaxin, which were not visible in the electron density maps. Crystallographic data and refinement statistics are given in Table S1. Note that the ordered region of the bound *N*-peptide of syntaxin 1 is slightly longer in *M. brevicollis* than in the Munc18-1/syntaxin 1a structure. A more detailed description of the *N*-peptide is given in Fig. S5.

domain and Glu166 of the linker helix in the *R. norvegicus* structure (Fig. S4). This is interesting as this interaction is thought to stabilize the closed conformation of rat syntaxin 1a. Notwithstanding, syntaxin 1 from *M. brevicollis* adopts a closed conformation in the Munc18/syntaxin 1 complex.

M. brevicollis Munc18 Controls SNARE Assembly. For many years, it has been known that tight binding of murine Munc18-1 to syntaxin 1a prevents syntaxin 1a from forming a SNARE complex (24, 25). Recently, we have discovered that binding of the syntaxin *N*-peptide to the outer surface of Munc18-1 can regulate this process: When the syntaxin 1a *N*-peptide is bound to Munc18-1, SNARE complex formation is slowed drastically, and removal of the *N*-peptide enables binding of syntaxin 1a to its partner SNAREs while still bound to Munc18-1 (23).

We therefore examined next whether this switch is present in the *M. brevicollis* Munc18–syntaxin 1 interaction as well. To monitor SNARE complex assembly, we established a fluorescence-based kinetic approach similar to the one that was instrumental to discovering the switch for the murine proteins (23). Indeed, when fluorescently labeled *M. brevicollis* synaptobrevin was mixed with SNAP-25 and syntaxin 1, with or without *N*-peptide, from *M. brevicollis*, an increase in fluorescence anisotropy corresponding to the formation of a ternary SNARE complex was observed. By contrast, premixing of Munc18 with Syx1 (1-279) produced an almost complete block of SNARE complex formation (Fig. 6*A, Left*). Remarkably, this block was not observed when Syx1 (20-279) was used instead (Fig. 6*A, Right*), demonstrating that binding of the *N*-peptide to Munc18 is required to block SNARE complex formation. Similar results were obtained when SNARE complex formation was monitored by SDS/PAGE (Fig. S6).

Discussion

It is widely accepted that zippering of SNARE proteins drives membrane fusion during neuronal exocytosis (15). By contrast, divergent models of how Munc18-1 interacts with the SNARE machinery have been proposed (19–21, 38). In recent years, a model is being favored, in which SM proteins generally clasp an assembled SNARE complex. This scenario seems to reconcile conflicting evidence from in vivo and in vitro studies because it places Munc18-1 at a central position at which it would be able to support membrane fusion. Although the scenario is tempting, it neglects the fact that the tight Munc18-1/syntaxin 1a complex interferes strongly with SNARE complex formation (23–25) and cannot explain how syntaxin 1 is able to escape the tight grip of Munc18. In addition, physiological investigations support a role for Munc18 upstream of the membrane fusion reaction (39).

Despite its extraordinarily stability, it has been argued that the binary Munc18-1/syntaxin 1a complex might only play a supporting role in neuronal secretion (e.g., refs. 20, 21, and 26). The strict structural and functional conservation of the Munc18/syntaxin 1 complex in *M. brevicollis*, however, brings now to light that the binary complex must have played an important role in the last common ancestor of choanoflagellates and animals and, hence, that it is not a specialization of the neuronal secretion apparatus. In fact, the binding mode with its two spatially separated but linked binding sites makes the binary complex perfectly suited for regulating an important step in the reaction cascade toward SNARE complex assembly (Fig. 6*B*).

Probably, the primordial machinery of the common ancestor of choanoflagellates and animals served as a starting point for the evolution of the more complex machinery found in animals, in particular in vertebrates. For example, we noted that a prominent expansion of the set of Munc18 genes took place during the evolution of vertebrates, giving rise to three different genes, Munc18-1, -2, and -3. Interestingly, a comparable expansion occurred in the set of secretory SNAREs during vertebrate
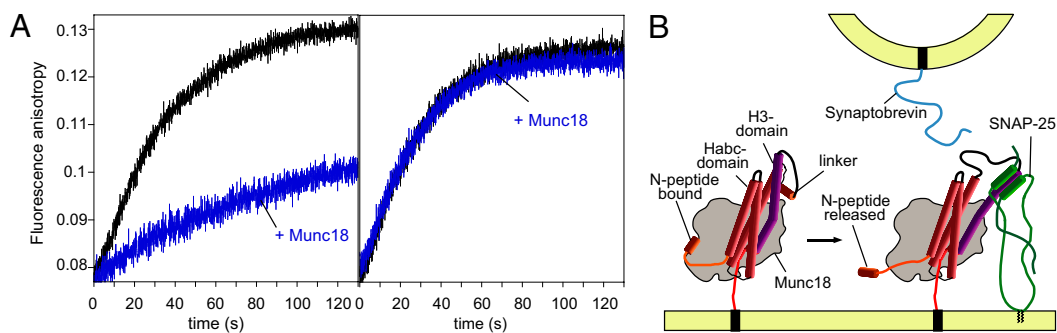
Fig. 6. Munc18 from *M. brevicollis* controls SNARE assembly. Synaptobrevin was labeled with Texas red at Cys58, corresponding to Cys79 of rat synaptobrevin 2 used in our previous study (23). Ternary SNARE complex formation was followed by the increase in fluorescence anisotropy of 50 nM fluorescent Syb1-75 upon mixing with 1 μM syntaxin 1 and 3 μM SNAP-25. In the absence of Munc18, SNARE complexes for both syntaxin 1 variants, Syx1 (1–279) and Syx1 (20–279) formed (*A*, black curves). In the presence of Munc18 (1 μM), SNARE assembly was almost completely inhibited for Syx 1 (1–279) (*Left*), but not for Syx1 (20–279) (*Right*). We noted that the slowdown of SNARE complex formation in the presence of Munc18-1 was not found when a semiquantitative binding assay was used (31). Therefore, it needs to be emphasized here that a kinetic approach is essential to uncover the switch mechanism, whereas binding assays, by nature, are often only suited to uncover an end-product of a binding reaction. (*B*) Schematic model of how the release of the *N*-peptide might set off a conformational change that allows binding of SNAP-25 to the Munc18/syntaxin 1 complex, in turn establishing a binding site for the vesicular synaptobrevin.

evolution (33), suggesting that distinct pairs of Munc18 and secretory syntaxins coevolved and may have helped develop a more versatile secretion apparatus. Indeed, those novel factors are largely confined to different subcellular locations or their expression is restricted to particular tissues or different developmental stages (15).

Remarkably, both rat and *M. brevicollis* syntaxin 1 adopt a closed conformation in complex with Munc18. At first glance, Munc18 appears to lock syntaxin into a conformation that is incompatible with SNARE complex assembly. Therefore, not surprisingly, it is often assumed that syntaxin first needs to leave the tight grip of Munc18. Only then, according to this idea, can syntaxin open up in preparation for SNARE complex assembly (19–21, 38). However, does syntaxin really need to escape to form a SNARE complex? An alternative explanation supported by our findings is that Munc18 might merely reorganize syntaxin in such a way that its conformation is compatible with SNARE complex assembly. Note that this conformation does not necessarily resemble the classical concept of an "open" syntaxin. In fact, we recently found that binding of the *N*-peptide to the outer surface of Munc18-1 is necessary for Munc18-1 to control the accessibility of syntaxin 1a for its SNARE partners. When syntaxin's *N*-peptide is removed, the block is relieved, suggesting that syntaxin 1a can form a SNARE complex while still bound to Munc18-1 (23). We found that this handover mechanism is also present in the homologous pair from *M. brevicollis*, demonstrating that it constitutes a fundamental functional principle of these proteins. It seems therefore that Munc18's essential role is to steer syntaxin into a configuration suited for SNARE complex assembly. How exactly this transition takes place, whether it involves a conformational change within the binary complex (Fig. 6*B*), and which other factors control this step will require further study.

Experimental Procedures

Protein Purification. The soluble portion of synaptobrevin [Syb (1-75)] was amplified by PCR from *M. brevicollis* cDNA. For specific labeling, a construct containing a cysteine at position 58 was prepared. Codon optimized version of SNAP-25 (1-210), Munc18 (1-649) and the soluble portion of syntaxin 1 [Syx1 (1-279)] of *M. brevicollis* were prepared by gene synthesis (GenScript). In addition, the following truncated variants were constructed: Syx1 (1-265); Syx1 (1-242); Syx1 (1-199); Syx1 (20-279), and Syx1 (200-279). All constructs were cloned into a pET28a vector and expressed in *E. coli*. Proteins and SNARE complexes assembled from purified monomers were purified by Ni²⁺-NTA affinity chromatography followed by ion-exchange chromatography essentially as described (23). A peptide comprising the first 20 residues of syntaxin 1 [Syx1 (1–20)] was synthesized (Biosyntan).

Phylogeny. Phylogenetic reconstruction was carried out as described (33). To gain insights into the phylogenetic placement of the core factors of the secretory machinery from the choanoflagellate *M. brevicollis*, we included sequences from 15 animals, 7 fungi, 6 plants, and 4 protists. Detailed information about the sequences and computational approaches used are given in *SI Experimental Procedures*.

ITC. ITC was performed on a VP-ITC instrument (GE Healthcare) at 25 °C essentially as described (23). The measured heat released on binding was integrated and analyzed with Microcal Origin 7.0 by using a single-site binding model, yielding the equilibrium association constant K_a, the enthalpy of binding ΔH, and the stoichiometry n. Experimental data are shown in Fig. S3.

Spectroscopy. Fluorescence measurements were carried out in a Fluorolog 3 spectrometer equipped for polarization (Horiba Scientific). All experiments were performed at 25 °C in 1-cm quartz cuvettetes in PBS buffer. Fluorescence anisotropy, which is used to indicate the local flexibility of the labeled residue, and which increases upon complex formation and decreases upon dissociation, were measured essentially as described (23). CD spectroscopy measurements were performed essentially as described (40, 41) by using the Chirascan instrument (Applied Photophysics). Quartz cuvettetes with a pathlength of 0.1 cm were used. The ellipticity at 222 nm was recorded between 20 and 95 °C at a temperature increment of 30 °C/h.

Crystallization and Data Collection. For crystallization, a slightly shorter syntaxin 1 construct, Syx1 (1-265), was used. This construct comprises the syntaxin region structured in the homologous Munc18-1/syntaxin 1a crystal structure, i.e., Syx1a (1-248) (23, 42). Syx1 (1-265) was found to bind Munc18 with the same affinity and enthalpy as Syx1 (aa 1–279) (Table 1 and Fig. S3). Crystals were obtained by the sitting drop vapor diffusion method by mixing equal volumes of 17 mg/mL Munc18/Syx1 (1-265) complex with reservoir buffer containing 7.5% PEG 6000 and 0.1 M Tris·HCl at pH 7.0, 4.25% 2-Methyl-2,4-Pentanediol and 15% glycerol. After flash-cooling in liquid nitrogen, diffraction data were collected to a resolution of 2.8 Å at SLS beamline PX2. The crystals belonged to space group P6₅22 with lattice dimensions of $a = b = 146.2$ Å and $c = 214.8$ Å. Procedures for structure determination and refinement are given in *SI Experimental Procedures*.

Cell culture and Microscopy. *M. brevicollis* (50154; American Type Culture Collection) were cultured in artificial sea water mixed with Wards cereal grass medium in a 1:1 ratio, adjusted to a salt concentration of 53 mS/cm and sterile-filtered. Cultures were maintained at 25 °C and diluted 1:100 once a week. For immunofluorescence, the cells were grown to a density of 10⁶ to 10⁷ cells/mL and fixed by adding formaldehyde to a final concentration of 4%. Approximately 0.7 mL of the fixed culture was applied to poly-L-lysine-coated coverslips and left to sediment for 30 min. At room temperature, the coverslips were washed gently four times with PEM (100 mM Pipes at pH 6.9, 1 mM EGTA, and 0.1 mM MgSO₄), incubated for 30 min in blocking solution (PEM+: 1% BSA, 0.3% Triton X-100), 1 h in primary antibodies solution (in PEM+), and after further washes (PEM+), 1 h in the dark with fluorescent

secondary antibodies (1:100 in PEM+, polyclonal goat anti-mouse-Cy2, and goat anti-rabbit-Cy5; Jackson Immunoresearch) and washed again four times (PEM). A last 15-min incubation in the dark with rhodamine phalloidin (6 U/ml in PEM; Molecular Probes) enabled the visualization of F-actin. After 3 washes (PEM), coverslips were mounted onto slides with Fluorescent Mounting Media (4 μL; Dako). The following primary antibodies have been used: mouse monoclonal antibody against β-tubulin (E7, 1:200; Developmental Studies Hybridoma Bank); rabbit polyclonals against *M. brevicollis* synaptobrevin (1:100), rat SNAP25 (1:200), rat syntaxin 1 (1:200), and rat Munc18 (1:200). Single-plane confocal images were taken under an inverted TCS-SP2 confocal laser-scanning microscope (Leica Microsystems) with a 63× (NA 1.4) oil objective and a digital zoom factor of 6. Confocal images from dual-labeling experiments were acquired in sequential scanning mode to avoid cross-talk/bleed-through between channels. For electron microscopy, cells were flash-frozen in a Baltec HPM 010 high-pressure freezer (Leica Microsystems). Cryosubstitution and embedding were performed in a Leica EM AFS as described (43). Briefly, specimens were sequentially incubated at low temperature (−90 °C) in 0.1% tannic acid (100 h) and 2% OsO_4 (7 h) in acetone. They were progressively brought to room temperature before being embedded in Epon (Electron Microscopy Sciences) and polymerized 24 h at 60 °C. Ultrathin sections were cut and contrasted with uranyl acetate and lead citrate before being observed in a LEO 912 AB (Zeiss).

See *SI Experimental Procedures* for additional materials and methods.

1. Putnam NH, et al. (2007) Sea anemone genome reveals ancestral eumetazoan gene repertoire and genomic organization. *Science* 317:86−94.
2. Chapman JA, et al. (2010) The dynamic genome of Hydra. *Nature* 464:592−596.
3. Srivastava M, et al. (2010) The Amphimedon queenslandica genome and the evolution of animal complexity. *Nature* 466:720−726.
4. Srivastava M, et al. (2008) The Trichoplax genome and the nature of placozoans. *Nature* 454:955−960.
5. King N (2004) The unicellular ancestry of animal development. *Dev Cell* 7:313−325.
6. Maldonado M (2004) Choanoflagellates, choanocytes, and animal multicellularity. *Invertebr Biol* 123:1−22.
7. Leadbeater B (2008) Choanoflagellate evolution: The morphological perspective. *Protistology* 5:256−267.
8. King N, et al. (2008) The genome of the choanoflagellate Monosiga brevicollis and the origin of metazoans. *Nature* 451:783−788.
9. Clarke HJ (1866) Conclusive proofs of the animality of the ciliate sponges, and of their affinities with the infusoria flagellata. *Am J Sci* 2:320−325.
10. Wainright PO, Hinkle G, Sogin ML, Stickel SK (1993) Monophyletic origins of the metazoa: An evolutionary link with fungi. *Science* 260:340−342.
11. Lang BF, O'Kelly C, Nerad T, Gray MW, Burger G (2002) The closest unicellular relatives of animals. *Curr Biol* 12:1773−1778.
12. Nielsen C (2008) Six major steps in animal evolution: Are we derived sponge larvae? *Evol Dev* 10:241−257.
13. Carr M, Leadbeater BS, Hassan R, Nelson M, Baldauf SL (2008) Molecular phylogeny of choanoflagellates, the sister group to Metazoa. *Proc Natl Acad Sci USA* 105:16641−16646.
14. Ryan TJ, Grant SGN (2009) The origin and evolution of synapses. *Nat Rev Neurosci* 10:701−712.
15. Jahn R, Scheller RH (2006) SNAREs–engines for membrane fusion. *Natl Rev* 7:631−643.
16. Hosono R, et al. (1992) The unc-18 gene encodes a novel protein affecting the kinetics of acetylcholine metabolism in the nematode Caenorhabditis elegans. *J Neurochem* 58:1517−1525.
17. Schulze KL, et al. (1994) rop, a Drosophila homolog of yeast Sec1 and vertebrate n-Sec1/Munc-18 proteins, is a negative regulator of neurotransmitter release in vivo. *Neuron* 13:1099−1108.
18. Verhage M, et al. (2000) Synaptic assembly of the brain in the absence of neurotransmitter secretion. *Science* 287:864−869.
19. Toonen RF, Verhage M (2007) Munc18-1 in secretion: Lonely Munc joins SNARE team and takes control. *Trends Neurosci* 30:564−572.
20. Rizo J, Rosenmund C (2008) Synaptic vesicle fusion. *Nat Struct Mol Biol* 15:665−674.
21. Südhof TC, Rothman JE (2009) Membrane fusion: Grappling with SNARE and SM proteins. *Science* 323:474−477.
22. Carr CM, Rizo J (2010) At the junction of SNARE and SM protein function. *Curr Opin Cell Biol* 22:488−495.
23. Burkhardt P, Hattendorf DA, Weis WI, Fasshauer D (2008) Munc18a controls SNARE assembly through its interaction with the syntaxin N-peptide. *EMBO J* 27:923−933.
24. Pevsner J, et al. (1994) Specificity and regulation of a synaptic vesicle docking complex. *Neuron* 13:353−361.
25. Yang B, Steegmaier M, Gonzalez LC, Jr., Scheller RH (2000) nSec1 binds a closed conformation of syntaxin1A. *J Cell Biol* 148:247−252.
26. Shen J, Tareste DC, Paumet F, Rothman JE, Melia TJ (2007) Selective activation of cognate SNAREpins by Sec1/Munc18 proteins. *Cell* 128:183−195.
27. Deák F, et al. (2009) Munc18-1 binding to the neuronal SNARE complex controls synaptic vesicle priming. *J Cell Biol* 184:751−764.
28. Peng RW, Guetg C, Abellan E, Fussenegger M (2010) Munc18b regulates core SNARE complex assembly and constitutive exocytosis by interacting with the N-peptide and the closed-conformation C-terminus of syntaxin 3. *Biochem J* 431:353−361.
29. Latham CF, et al. (2006) Molecular dissection of the Munc18c/syntaxin4 interaction: Implications for regulation of membrane trafficking. *Traffic* 7:1408−1419.
30. Hu SH, Latham CF, Gee CL, James DE, Martin JL (2007) Structure of the Munc18c/Syntaxin4 N-peptide complex defines universal features of the N-peptide binding mode of Sec1/Munc18 proteins. *Proc Natl Acad Sci USA* 104:8773−8778.
31. Hu SH, et al. (2011) Possible roles for Munc18-1 domain 3a and Syntaxin1 N-peptide and C-terminal anchor in SNARE complex formation. *Proc Natl Acad Sci USA* 108:1040−1045.
32. Hashizume K, Cheng YS, Hutton JL, Chiu CH, Carr CM (2009) Yeast Sec1p functions before and after vesicle docking. *Mol Biol Cell* 20:4673−4685.
33. Kloepper TH, Kienle CN, Fasshauer D (2008) SNAREing the basis of multicellularity: Consequences of protein family expansion during evolution. *Mol Biol Evol* 25:2055−2068.
34. Leadbeater B, Kelly M (2001) Evolution of animals-choanoflagellates and sponges. *Water and Atmosphere* 9:9−11.
35. Laval M (1971) Ultrastructure and feeding mode of the choanoflagellate Salpinogoeca pelagica sp. nov. - comparison with sponge choanocytes (Translated from French). *Protistologica* 7:325−336.
36. Karpov S, Leadbeater B (1998) Cytoskeleton structure and composition in choanoflagellates. *J Eukaryot Microbiol* 45:361−367.
37. Hayashi T, et al. (1994) Synaptic vesicle membrane fusion complex: Action of clostridial neurotoxins on assembly. *EMBO J* 13:5051−5061.
38. Carr CM, Rizo J (2010) At the junction of SNARE and SM protein function. *Curr Opin Cell Biol* 22:1−8.
39. Gulyás-Kovács A, et al. (2007) Munc18-1: Sequential interactions with the fusion machinery stimulate vesicle docking and priming. *J Neurosci* 27:8676−8686.
40. Wiederhold K, Fasshauer D (2009) Is assembly of the SNARE complex enough to fuel membrane fusion? *J Biol Chem* 284:13143−13152.
41. Fasshauer D, Antonin W, Subramaniam V, Jahn R (2002) SNARE assembly and disassembly exhibit a pronounced hysteresis. *Nat Struct Biol* 9:144−151.
42. Misura KM, Scheller RH, Weis WI (2000) Three-dimensional structure of the neuronal-Sec1-syntaxin 1a complex. *Nature* 404:355−362.
43. Möbius W, et al. (2010) Electron microscopy of the mouse central nervous system. *Methods Cell Biol* 96:475−512.

Supporting Information

Burkhardt et al. 10.1073/pnas.1106189108

SI Experimental Procedures

Structure Determination and Refinement. Diffraction data were integrated and scaled with XDS (1). The structure was solved by molecular replacement using Phaser (2). The search model was generated by pruning nonconserved residues of the neuronal Munc18-1/syntaxin 1a complex (PDB ID code 3C98; ref. 3) to alanines with Chainsaw (4). The asymmetric unit contains one Munc18/syntaxin 1 complex. The model was refined by using simulated annealing, gradient minimization, and individual isotropic B-factor refinement as implemented in Phenix (5) alternated by rebuilding cycles using the program Coot (6). In a final step, tensor elements describing the anisotropic displacement of four individual domains of Munc18 and four regions of syntaxin 1 were refined by using the Translation/Libration/Screw (TLS) implementation of Phenix. The final R factor is 0.188 with a R_{free} of 0.258. The final model comprises Munc18 residues 1–509 and 561–616, syntaxin 1 residues 2–15, 39–192, and 210–261, and 48 water molecules (Table S1). Figures were generated with the program Pymol (7). The coordinates have been deposited in the RCSB Protein Data Bank (ID code 2XHE) and will be released upon publication.

Phylogeny. Phylogenetic reconstruction was essentially done as described in ref. 8. To gain insights into the phylogenetic placement of the core factors of the secretory machinery from the choanoflagellate *M. brevicollis*, we included sequences from 15 selected animal species, 7 selected fungal species, 6 selected plant species, and 3 protists for the construction of the phylogenetic trees. The sequences of the secretory SNARE proteins (i.e., type IV) were downloaded from our SNARE database http://bioinformatics.mpibpc.mpg.de/snare. The sequences of the secretory SM proteins were gathered from the nr-database at National Center for Biotechnology Information and few genome projects from the Department of Energy Joint Genome Institute. The species list and abbreviations and the sequence identity

numbers of the used sequences can be found in Table S2 and Table S3. We then aligned each factor by using muscle (9).

Phylogenetic reconstruction was composed of two different analytical approaches. The first approach used Important Quartet Puzzling and Nearest Neighbor Interchange (IQPNNI) (10) to construct phylogenetic trees from the curated alignments. We used a gamma distribution as a model for rate heterogeneity with four rate categories for the estimation of the gamma distribution parameter. The proportion of invariable sites was estimated from the data and the Jones, Taylor, and Thornton (JTT) distance matrix (11) served as a substitution matrix. We used the stopping rule of IQPNNI, but the calculation had to run for at least the suggested number of iterations. The default values were used for the remaining parameter. In addition, likelihood mapping was applied to determine the confidence of the edges in the calculated trees. The second approach used the phylip package (12) to apply a distance-based bootstrap analysis with 1,000 replicates to each of the curated alignments. Standard settings were used for seqboot, the JTT distance matrix, and also a gamma distribution (with parameter approximation from tree puzzle) for protdist, as were standard options for neighbor. If required, the random seed was set to nine. We used the almost unbiased (AU) test (13) to address the systematically biased bootstrap values. We obtained the sitewise log-likelihoods needed for the AU test by using a modified version of phyml (14), and the test was performed by using consel (15). The reconstructed IQPNNI trees served as starting points to join the results of both calculations. The inner edges of the trees were labeled with their likelihood mapping and corrected bootstrap support values.

Electrophoretic Procedures. SDS resistance of ternary SNARE complexes in polyacrylamide gels (16) was tested as described (17) with the modification that the complexes were visualized by the incorporation of synaptobrevin (1-75) labeled with the fluorescent dye Texas red at cysteine 58.

1. Kabsch W (1993) Automatic processing of rotation diffraction data from crystals of initially unknown symmetry and cell constants. *J Appl Cryst* 26:795–800.
2. McCoy AJ, Grosse-Kunstleve RW, Storoni LC, Read RJ (2005) Likelihood-enhanced fast translation functions. *Acta Crystallogr D Biol Crystallogr* 61:458–464.
3. Burkhardt P, Hattendorf DA, Weis WI, Fasshauer D (2008) Munc18a controls SNARE assembly through its interaction with the syntaxin N-peptide. *EMBO J* 27:923–933.
4. Stein N (2008) CHAINSAW: A program for mutating pdb files used as templates in molecular replacement. *J Appl Cryst* 41:641–643.
5. Adams PD, et al. (2004) Recent developments in the PHENIX software for automated crystallographic structure determination. *J Synchrotron Radiat* 11:53–55.
6. Emsley P, Cowtan K (2004) Coot: Model-building tools for molecular graphics. *Acta Crystallogr D Biol Crystallogr* 60:2126–2132.
7. DeLano WL (2002) *The PyMOL Molecular Graphics System* (DeLano Scientific, Palo Alto, CA).
8. Kloepper TH, Kienle CN, Fasshauer D (2007) An elaborate classification of SNARE proteins sheds light on the conservation of the eukaryotic endomembrane system. *Mol Biol Cell* 18:3463–3471.
9. Edgar RC (2004) MUSCLE: A multiple sequence alignment method with reduced time and space complexity. *BMC Bioinformatics* 5:113.
10. Vinh S, Von Haeseler A (2004) IQPNNI: Moving fast through tree space and stopping in time. *Mol Biol Evol* 21:1565–1571.
11. Jones DT, Taylor WR, Thornton JM (1992) The rapid generation of mutation data matrices from protein sequences. *Comput Appl Biosci* 8:275–282.
12. Felsenstein J (1998) PHYLIP - Phylogeny inference package (Version 3.2). *Cladistics* 5: 164–166.
13. Shimodaira H (2002) An approximately unbiased test of phylogenetic tree selection. *Syst Biol* 51:492–508.
14. Guindon S, Gascuel O (2003) A simple, fast, and accurate algorithm to estimate large phylogenies by maximum likelihood. *Syst Biol* 52:696–704.
15. Shimodaira H, Hasegawa M (2001) CONSEL: For assessing the confidence of phylogenetic tree selection. *Bioinformatics* 17:1246–1247.
16. Hayashi T, et al. (1994) Synaptic vesicle membrane fusion complex: Action of clostridial neurotoxins on assembly. *EMBO J* 13:5051–5061.
17. Fasshauer D, Antonin W, Margittai M, Pabst S, Jahn R (1999) Mixed and non-cognate SNARE complexes. Characterization of assembly and biophysical properties. *J Biol Chem* 274:15440–15446.
18. Dulubova I, et al. (1999) A conformational switch in syntaxin during exocytosis: Role of munc18. *EMBO J* 18:4372–4382.
19. Misura KM, Scheller RH, Weis WI (2000) Three-dimensional structure of the neuronal-Sec1-syntaxin 1a complex. *Nature* 404:355–362.
20. Munson M, Chen X, Cocina AE, Schultz SM, Hughson FM (2000) Interactions within the yeast t-SNARE Sso1p that control SNARE complex assembly. *Nat Struct Biol* 7: 894–902.
21. Margittai M, et al. (2003) Single-molecule fluorescence resonance energy transfer reveals a dynamic equilibrium between closed and open conformations of syntaxin 1. *Proc Natl Acad Sci USA* 100:15516–15521.
22. Weimer RM, et al. (2006) UNC-13 and UNC-10/rim localize synaptic vesicles to specific membrane domains. *J Neurosci* 26:8040–8047.
23. Gerber SH, et al. (2008) Conformational switch of syntaxin-1 controls synaptic vesicle fusion. *Science* 321:1507–1510.
24. Hu SH, Latham CF, Gee CL, James DE, Martin JL (2007) Structure of the Munc18c/Syntaxin4 N-peptide complex defines universal features of the N-peptide binding mode of Sec1/Munc18 proteins. *Proc Natl Acad Sci USA* 104:8773–8778.
25. Hu SH, et al. (2011) Possible roles for Munc18-1 domain 3a and Syntaxin1 N-peptide and C-terminal anchor in SNARE complex formation. *Proc Natl Acad Sci USA* 108: 1040–1045.
26. Peng RW, Guetg C, Abellan E, Fussenegger M (2010) Munc18b regulates core SNARE complex assembly and constitutive exocytosis by interacting with the N-peptide and the closed-conformation C-terminus of syntaxin 3. *Biochem J* 431:353–361.
27. Lovell SC, et al. (2003) Structure validation by Calpha geometry: Phi,psi and Cbeta deviation. *Proteins* 50:437–450.

Fig. S1. Detailed versions of the phylogenetic trees of the SM protein Munc18 (*A*), the Qbc-SNARE SNAP-25 (*B*), and secretory syntaxins (*C*) (type Qa.IV) shown in Fig. 1. The major phylogenetic lineages are indicated by different colors. The labels on the major branches represent the likelihood mapping (left) and almost unbiased (AU) support values (right). The species abbreviations and sequences used are given in Table S2 and Table S3. Whereas *M. brevicollis* possesses only one factor each, duplications occurred recurrently in different animal lineages. A noteworthy expansion of Munc18-like factors occurred in vertebrates, giving rise to the three isoforms Munc18-1, -2, and -3. A more prominent expansion took place in secretory syntaxins in vertebrates (8). Interestingly, the SNAP-25–like protein found in *M. brevicollis* is closely related to the neuronal SNAP-25 of animals (8), whereas the sequences of the other two Qbc-SNAREs animal homologs SNAP-29 and SNAP-47, have diverged substantially.

Fig. S2. Change of intrinsic fluorescence upon binding of Munc18 to syntaxin 1 (*A*) and overlay of the Munc18/Syx1 complexes (*B*). (*A*) Baseline corrected tryptophan fluorescence emission spectra of Syx1 (1-279), Munc18, Munc18 mixed with Syx1 (1-279), and Munc18 mixed with Syx1 (20-279) (500 nM each) after excitation at 295 nm. Upon addition of Syx1 (1-279) or Syx1 (20-279) to Munc18-1, an increase in fluorescence was monitored. Note that syntaxin 1 does not posses a tryptophan. Interestingly, the increase in tryptophan fluorescence in the presence of Syx1 (20-279) was somewhat less pronounced than in the presence of Syx1 (1-279). A similar difference in the fluorescence change was observed for the rat homologs. This change in fluorescence suggests that both syntaxin variants adopt a slightly different conformation in complex with Munc18. It seems likely that the increase in tryptophan fluorescence is caused by close proximity of Trp-24 of *M. brevicollis* Munc18 (Trp-28 of rat Munc18-1) and Phe-46 and Phe-47 of *M. brevicollis* syntaxin 1 (Phe-33 and Phe-34 of rat Syx1a). (*B*) Overlay of the Munc18/Syx1 complexes from *M. brevicollis* (Munc18, blue; Syx1, red) and from *R. norvegicus* (Munc18-1, light blue; Syx1a, salmon; PDB ID code 3C98) reveals their overall similarity.

Fig. S3. Isothermal titration calorimetry data for the interaction of syntaxin 1 and Munc18. All isothermal calorimetric experiments were performed at 25 °C in PBS buffer. In each titration, the syntaxin 1 variant or syntaxin 1 assembled into a purified ternary SNARE complex was injected into Munc18 from *M. brevicollis* or Munc18-1 from *Rattus norvegicus* (*Bottom*). In each graph, *Upper* shows the base-line corrected raw data in power versus time during the injections. *Lower* displays the integrated areas normalized to the amount of the injectant (kcal·mol^{-1}) versus its molar ratio to Munc18. The solid lines represent the best fit to the data for a single binding site model by using a nonlinear least squares fit. The results of the fits are given in Table 1. For experiments performed in replicate, a representative example is shown. Most titrations using individual syntaxin 1 variants were carried out at 20 μM syntaxin 1 and 2.5 μM Munc18. A higher concentration was used (50 μM and 4 μM, respectively) for Syx1 (1-242) and (40 μM and 4 μM, respectively) for Syx1 (1-199) to account for the smaller heat changes upon interaction with Munc18. Similarly, 30 μM and 3.5 μM, respectively, were used for titrating purified SNARE complexes and Munc18.
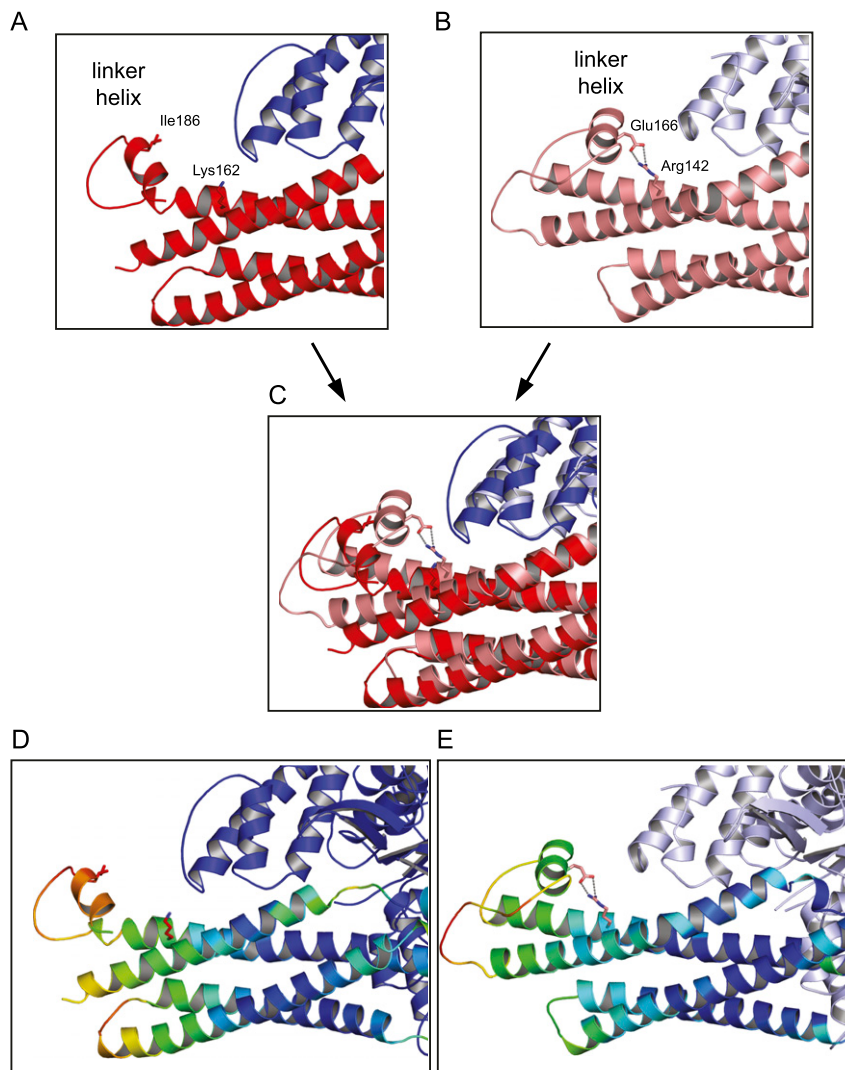
Fig. S4. Different conformations of the linker helix in the Munc18/syntaxin 1 complexes from *Monosiga brevicollis* and *Rattus norvegicus*. Different conformation of the linker helix of syntaxin1 from *M. brevicollis* (*A*) and from *R. norvegicus* (PDB ID code 3C98; ref. 3) (*B*). An overlay of the two structures is shown in *C*. In the structure from *R. norvegicus,* the orientation of the linker helix of syntaxin 1a is stabilized by the residues Glu166 of the linker helix and Arg142 of the Hb helix. This interaction is thought to stabilize the closed conformation of syntaxin 1a (18, 19). In the *M. brevicollis* structure, the corresponding residues, Ile186 and Lys162, do not interact. Nevertheless, syntaxin 1 from *M. brevicollis* adopts a closed conformation in the Munc18/syntaxin 1 complex. Interestingly, the linker of *M. brevicollis* syntaxin appears to be slightly more flexible compared with the one of rat. In fact, we observed that residues of the linker helix exhibit elevated temperature factors compared with the rest of the model (*D*), whereas the residues of the linker helix of the structure from *R. norvegicus* do not display elevated temperature factors (*E*). This difference possibly explains why the block of SNARE assembly exerted by Munc18 from *M. brevicollis* is somewhat less efficient than observed for the vertebrate homologs. Incidentally, the yeast syntaxin Sso1 has been found in a tight closed conformation in the absence of its SM partner Sec1 (20). Sso1's closed conformation is stabilized by multiple intermolecular contacts, whereas the closed conformation of syntaxin 1 of *R. norvegicus* and of *M. brevicollis* appears to be reinforced by Munc18. In fact, in isolation, rat syntaxin 1 rapidly switches between an open and closed conformation, with the majority of molecules being open (21). Of note, a double mutation in the aforementioned linker region, L165A/E166A (Syx1a[LE]) was used in several studies. Because this mutation was originally proposed to open up syntaxin 1a (18), it was anticipated that it would not require the activity of Munc18. Unexpectedly, however, Syx1[LE] turned out to be unable to bypass the requirement for Unc18 in *C. elegans* (22). Remarkably, Munc18a-1 nonetheless tightly enfolds Syx1a[LE] (3), presumably in a closed conformation, yet is unable to stop it from forming a SNARE complex. It seems possible that Syx1a[LE] in complex with Munc18 adopts a less rigid closed conformation, which permits SNARE complex assembly independent of whether its *N*-peptide is bound to the outer surface of Munc18-1 (3). The less rigid closed conformation is supported by the somewhat smaller intrinsic fluorescence change observed for the mutant upon binding to Munc18-1 (3). In this context. it is interesting to note that knockout/knockin mice that express only Syx1b[LE] showed an enhanced fusogenicity of synaptic vesicles (23), supporting the view that Munc18-1 lost some of its control over the accessibility of syntaxin.
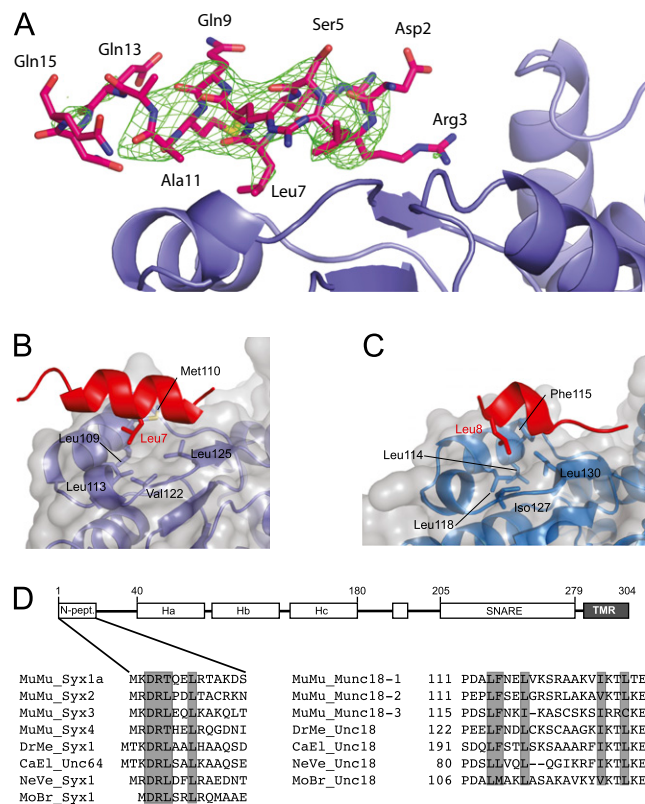
Fig. S5. The syntaxin 1 *N*-peptide binds to the outer surface of Munc18. (*A*) F_{obs}-F_{calc} omit map of the *M. brevicollis* Syx1 *N*-peptide region contoured at 3σ (green mesh). The final model is shown as sticks (carbon: pink). Blue: *M. brevicollis* Munc18 displayed as cartoon. (*B* and *C*) Detailed view on the *N*-peptide binding pocket of the choanoflagellate and the vertebrate Munc18/syntaxin 1 complex. In *M. brevicollis*, Leu7 packs into a hydrophobic pocket formed by the residues Leu109, Met110, Leu113, Val122, and Leu125 of Munc18. The *N*-peptide is shown in red and domain 1 of Munc18 in blue (*B*). In *R. norvegicus*, the corresponding residue Leu8 sandwiches into the homologous hydrophobic pocket formed by the residues Leu114, Phe115, Leu118, Ile127, and Leu130. Interestingly, the ordered region of the bound *N*-peptide of syntaxin 1 is slightly longer in *M. brevicollis* (comprising residues 2–15) as in the Munc18-1-syntaxin 1a structure (residues 2–9). The overall structure of the bound syntaxin 1 *N*-peptide is similar to that of syntaxin 4 bound to Munc18-3 (24, 25), but note that so far no structure of Munc18-3 with the remainder of syntaxin 4 is available. When comparing the structure and working of the orthologous Munc18/syntaxin pairs of vertebrates, it should also be kept in mind that all three Munc18 orthologs in vertebrates originate from a single gene. Likewise, the different secretory syntaxins of vertebrates arose from gene duplications during the rise of vertebrates, suggesting that they function similarly (see, for example, ref. 26). (*D*) Schematic drawing of the domain structure of *M. brevicollis* syntaxin 1. Sequence alignments of the *N*-peptide of syntaxin (*Left*) and of the conserved *N*-peptide binding site in Munc18 (*Right*) from mice, fly, nematode, sea anemone, and choanoflagellate are shown. Note that the *N*-peptide of syntaxin 1 from *M. brevicollis* possesses a highly conserved DRL/TxxL-motif.
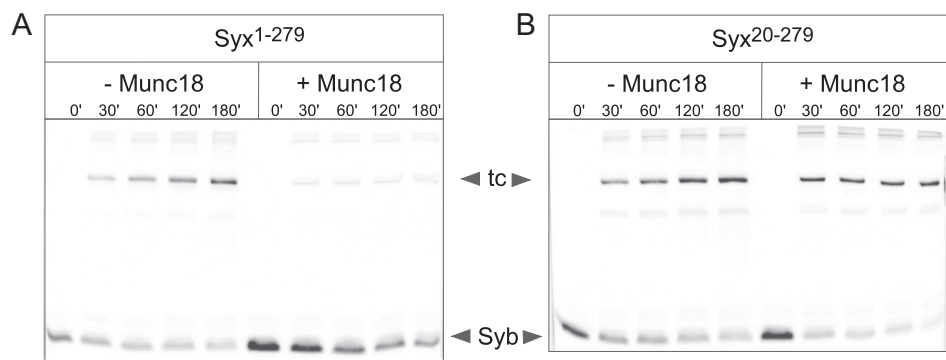

Fig. S6. Assembly of SDS-resistant SNARE complexes for syntaxin with (Syx1-279) and without *N*-peptide (Syx20-279) in the absence or presence of Munc18. Assembly of SNARE complexes in the absence or presence of Munc18 was monitored by the formation of SDS-resistant complexes (tc) containing synaptobrevin labeled with the fluorescent dye Texas red at Cys58. For both syntaxin 1 variants, Syx1 (1-279) and Syx1 (20-279), SNARE complexes formed in the absence of Munc18. In the presence of Munc18, however, SNARE complex formation was inhibited for Syx1 (1-279) (*A*), whereas a clear SDS-resistant band was visible for Syx1 (20-279) (*B*).

Table S1. Crystallographic data and refinement statistics

Measurement	Value
Wavelength, Å	1.0385
Temperature, K	100
Space group	$P6_522$
Unit cell parameters, Å	
a, b	146.2
c	214.8
Resolution, Å	35.0–2.8 (2.9–2.8)
Reflections	
Unique	30,089
Completeness, %	99.9 (100)
Redundancy	14.7 (14.3)
Mean $I/\sigma(I)$	19.8 (2.1)
$R_{sym}(I)$*, %	10.0 (75.4)
Refinement	
Resolution, Å	35.0–2.8
Reflections	
Number	30,041
Completeness, %	99.9
Test set, %	5
R_{work}[†], %	18.8
R_{free}[†], %	25.0
ESU, Å	0.39
Contents of A.U.	
Complexes/protein molecules/residues/ atoms	1/2/835/6,315
Water oxygens	48
Mean B factors, Å^2	
Wilson	75.2
Protein	104.8
Water	70.8
Ramachandran plot[‡], %	
Preferred	89.3
Allowed	8.7
Disallowed	2.0
rmsd from target geometry	
Bond lengths, Å	0.007
Bond angles, °	1.069
Chirality, Å	0.075
Dihedral angles, °	18.07
PDB ID code	2XHE

Data for the highest resolution shell in parentheses. ESU, estimated overall coordinate error based on maximum likelihood; A.U., asymmetric unit; rmsd, root-mean-square deviation.

*$R_{sym}(I) = \Sigma_{hkl}\Sigma_i|I_i(hkl) - <I(hkl)>|/\Sigma_{hkl}\Sigma_i|I_i(hkl)|$; for n independent reflections and i observations of a given reflection; $<I(hkl)>$ – average intensity of the i observations.

[†]$R = \Sigma_{hkl}||F_{obs}| - |F_{calc}||/\Sigma_{hkl}|F_{obs}|$; R_{work}, hkl $\notin$ T; R_{free}, hkl $\in$ T; R_{all}, all reflections; T, test set.

[‡]According to ref. 27.

Table S2.   Species list and abbreviations

Species	Abbreviation
Amphimedon queenslandica	AmQu
Arabidopsis thaliana	ArTh
Branchiostoma floridae	BrFl
Caenorhabditis elegans	CaEl
Capitella sp. 1	CaSp
Chlamydomonas reinhardtii	ChRe
Chlorella sp. NC64A	ChSp
Ciona intestinalis	CiIn
Danio rerio	DaRe
Drosophila melanogaster	DrMe
Entamoeba dispar SAW760	EnDi
Entamoeba histolytica HM-1:IMSS	EnHi
Gallus gallus	GaGa
Hellobdella robusta	HeRo
Homo sapiens	HoSa
Hydra magnipapillata	HyMa
Laccaria bicolor S238N-H82	LaBi
Lottia gigantea	LoBi
Magnaporthe grisea 70–15	MaGr
Micromonas sp. RCC299	MiSt
Monosiga brevicollis	MoBr
Mus musculus	MuMu
Nematostella vectensis	NeVe
Neurospora crassa N150	NeCr
Ostreococcus tauri	OsTa
Saccharomyces cerevisiae	SaCe
Schizosaccharomyces pombe	ScPo
Trichoplax adhaerens	TrAd
Trypanosoma brucei TREU927	TrBr
Ustilago maydis 521	UsMa
Volvox carteri f. nagariensis	VoCa
Yarrowia lipolytica CLIB99	YaLi

Table S3. Identity of used sequences

Name	Species	Database source	Identification no.
Secretory SM proteins			
HoSa_Munc18_1a	*Homo sapiens*	NCBI_nr	4507297
CaEl_Unc18	*Caenorhabditis elegans*	NCBI_nr	71988800
GaGa_Munc18_1	*Gallus gallus*	NCBI_nr	46195820
MuMu_Munc18_2	*Mus musculus*	NCBI_nr	6755688
TrBr_Sec1	*Trypanosoma brucei* TREU927	NCBI_nr	71744018
MiSt_Sec1	*Micromonas* sp. RCC299	NCBI_nr	255089845
HeRo_Unc18_2	*Hellobdella robusta*	DOE JGI	Helro1|187018
LoGi_Unc18	*Lottia gigantea*	DOE JGI	Lotgi1|237771
EnDi_Sec1_part	*Entamoeba dispar* SAW760	NCBI_nr	167384806
DaRe_Munc18_2	*Danio rerio*	NCBI_nr	47086919
VoCa_Sec1	*Volvox carteri* f. nagariensis	DOE JGI	Volca1|67807
GaGa_Munc18_3	*Gallus gallus*	NCBI_nr	119331098
BrFl_Unc18	*Branchiostoma floridae*	NCBI_nr	219459049
AmQu_Unc18	*Amphimedon queenslandica*	Compagen, Assembled by hand	
NeVe_Unc18	*Nematostella vectensis*	NCBI_nr	156390747
NeCr_Sec1	*Neurospora crassa* N150	NCBI_nr	85108189
ArTh_Sec1	*Arabidopsis* thaliana	NCBI_nr	18391384
HyMa_Unc18	*Hydra magnipapillata*	NCBI_nr	221121424
SaCe_Sec1	*Saccharomyces cerevisiae*	NCBI_nr	6320368
MaGr_Sec1	*Magnaporthe grisea* 70–15	NCBI_nr	145612411
LaBi_Sec1	*Laccaria bicolor* S238N-H82	NCBI_nr	170087878
DrMe_Unc18	*Drosophila melanogaster*	NCBI_nr	24657265
ArTh_Sec1_4	*Arabidopsis thaliana*	NCBI_nr	7267913
EnHi_Sec1	*Entamoeba histolytica* HM-1:IMSS	NCBI_nr	56464018
MuMu_Munc18_1a	*Mus musculus*	NCBI_nr	165972307
TrAd_Unc18	*Trichoplax adhaerens*	NCBI_nr	196000262
ChSp_Sec1	*Chlorella* sp. NC64A	DOE JGI	ChlNC64A_1|56812
ScPo_Sec1	*Schizosaccharomyces pombe*	NCBI_nr	19075726
DaRe_Munc18_3	*Danio rerio*	NCBI_nr	47087331
UsMa_Sec1	*Ustilago maydis* 521	NCBI_nr	71019769
ChRe_Sec1	*Chlamydomonas reinhardtii*	NCBI_nr	158273495
DaRe_Munc18_1	*Danio rerio*	NCBI_nr	68448507
MoBr_Munc18	*Monosiga brevicollis* MX1	NCBI_nr	167523609
HoSa_Munc18_3	*Homo sapiens*	NCBI_nr	118600975
MuMu_Munc18_3a	*Mus musculus*	NCBI_nr	6755690
CiIn_Unc18	*Ciona intestinalis*	NCBI_nr	198429537
HoSa_Munc18_2a	*Homo sapiens*	NCBI_nr	188528689
NeVe_Unc18_2	*Nematostella vectensis*	NCBI_nr	156390749
ArTh_Sec1_3	*Arabidopsis thaliana*	NCBI_nr	18413751
ArTh_Sec1_2	*Arabidopsis thaliana*	NCBI_nr	145334974
CaSp_Unc18_1	*Capitella* sp. 1	DOE JGI	Capca1|150412
YaLi_Sec1	*Yarrowia lipolytica* CLIB99	NCBI_nr	50553686
HeRo_Unc18	*Hellobdella robusta*	DOE JGI	Helro1|66166
Qbc-SNARE			
MuMu_SN29	*Mus musculus*	NCBI_nr	31543752
LoGi_SN25	*Lottia gigantea*	DOE JGI	Lotgi1|197810
HeRo_SN25-2	*Hellobdella robusta*	DOE JGI	Helro1|71107
GaGa_SN23	*Gallus gallus*	NCBI_nr	50748211
HeRo_SN29	*Hellobdella robusta*	DOE JGI	Helro1|184904
UsMa_Sec9	*Ustilago maydis* 521	NCBI_nr	49072430
CaEl_SN25	*Caenorhabditis elegans*	NCBI_nr	32567202
HyMa_SN29	*Hydra magnipapillata*	NCBI_est	46968126
ArTh_SN33	*Arabidopsis thaliana*	NCBI_nr	15240163
GaGa_SN47	*Gallus gallus*	NCBI_nr	50732155
HoSa_SN29	*Homo sapiens*	NCBI_nr	4759154
DrMe_SN25	*Drosophila melanogaster*	NCBI_nr	1763657
BrFl_SN47	*Branchiostoma floridae*	DOE JGI	Brafl1|240128
MuMu_SN47	*Mus musculus*	NCBI_nr	21362303
MuMu_SN23	*Mus musculus*	NCBI_nr	6678049
TrAd_SN25-2	*Trichoplax adhaerens*	DOE JGI	Triad1|63490
HyMa_SNx	*Hydra magnipapillata*	NCBI_est	47136750
CaEl_SN29	*Caenorhabditis elegans*	NCBI_nr	17554000

Table S3.   Cont.

Name	Species	Database source	Identification no.
NeVe_SN29	*Nematostella vectensis*	DOE JGI	Nemve1|108962
GaGa_SN25b	*Gallus gallus*	NCBI_nr	45382033
CaSp_SN25	*Capitella* sp. 1	DOE JGI	Capca1|180292
HoSa_SN25a	*Homo sapiens*	NCBI_nr	18765733
ArTh_SN30	*Arabidopsis thaliana*	NCBI_nr	15222976
HeRo_SN25	*Hellobdella robusta*	DOE JGI	Helro1|155336
LoGi_SN29	*Lottia gigantea*	DOE JGI	Lotgi1|237114
LoGi_SN47	*Lottia gigantea*	DOE JGI	Lotgi1|172501
BrFl_SN29	*Branchiostoma floridae*	NCBI_est	66378306
TrAd_SN47p	*Trichoplax adhaerens*	DOE JGI	Triad1|55100
CaSp_SN29	*Capitella* sp. 1	DOE JGI	Capca1|19521
DrMe_SN24	*Drosophila melanogaster*	NCBI_nr	17737875
AmQu_SN25	*Amphimedon queenslandica*	Compagen, Assembled by hand	
NeVe_SN47	*Nematostella vectensis*	NCBI, Assembled by hand	
TrAd_SN25	*Trichoplax adhaerens*	DOE JGI	Triad1|51809
CiIn_SN25	*Ciona intestinalis*	DOE JGI	Cioin2|294632
BrFl_SN25	*Branchiostoma floridae*	NCBI_est	66384552
BrFl_SN25like	*Branchiostoma floridae*	DOE JGI	Brafl1|84606
CiIn_SN29	*Ciona intestinalis*	DOE JGI	Cioin2|275649
HoSa_SN47	*Homo sapiens*	NCBI_nr	37589927
SaCe_Sec9	*Saccharomyces cerevisiae*	NCBI_nr	6321446
EnDi_SNp	*Entamoeba dispar* SAW760	NCBI_nr	167395986
DaRe_SN23	*Danio rerio*	NCBI_nr	41055690
MoBr_SN25	*Monosiga brevicollis*	DOE JGI	JGI_XYM16904.rev
HoSa_SN25b	*Homo sapiens*	NCBI_nr	18765735
ShPo_Sec9	*Schizosaccharomyces pombe*	NCBI_nr	19113435
DaRe_SN29	*Danio rerio*	NCBI_nr	63102202
DaRe_SN25a	*Danio rerio*	NCBI_nr	37589801
NeVe_SN25	*Nematostella vectensis*	DOE JGI	Nemve1|229104
HoSa_SN23	*Homo sapiens*	NCBI_nr	18765729
ChRe_SN29	*Chlamydomonas reinhardtii*	DOE JGI	Chlre3|155582
GaGa_SN29	*Gallus gallus*	NCBI_nr	50756211
MuMu_SN25a	*Homo sapiens*	NCBI_nr	54696236
EnDi_SnpOrNpsn	*Entamoeba dispar* SAW760	NCBI_nr	165893407
MuMu_SN25b	*Mus musculus*	NCBI_nr	6755588
DaRe_SN25b	*Danio rerio*	NCBI_nr	70887763
VoCa_SN29	*Volvox carteri* f. nagariensis	DOE JGI	Volca1|104786
SaCe_Spo20	*Saccharomyces cerevisiae*	NCBI_nr	6323659
ArTh_SN29	*Arabidopsis thaliana*	NCBI_nr	15241436
DaRe_SN47	*Danio rerio*	NCBI_nr	68404785
OsTa_SN25	*Ostreococcus tauri*	DOE JGI	Ostta4|36669
MaGr_Sec9	*Magnaporthe grisea* 70–15	NCBI_nr	38101969
YaLi_Sec9	*Yarrowia lipolytica* CLIB99	NCBI_nr	50553382